ARTICLE

Synthetic Textiles Processed Using Ionized Gas for Exterior Uses

Noam W Buckley [1,*]

[1] University of Miami

Abstract

In this paper, with the goal of preparing flexible gas sensors that can be worn externally, gas-sensitive materials were combined with flexible textile substrates to endow the gas sensors with weavability. The MAX phase was etched by LiF/HCl method to prepare the oligolayer $Ti_3C_2T_x$. Electrostatic spinning technique combined with hydrothermal method was used to obtain the TPU precursor solution to prepare the TPU fiber mat, which was used as the substructure of the flexible sensor. Then the $Ru/TiO_2/Ti_3C_2T_x$ flexible multifunctional sensor was prepared by attaching the material to the TPU fiber mat through high-power ultrasonic treatment. The sample fibers were structurally characterized using XRD and SEM, and the gas-sensitive and mechanical properties of the sample sensors were tested.SEM analyses showed that the surface of the TPU/ $Ru/TiO_2/Ti_3C_2T_x$ fibers was rough, and the composite material completely covered the surface of the TPU, and the chemical force between the material and the fiber mats made a tight connection, which provided an electrically conductive pathway for the sensor. The $Ru/TiO_2/Ti_3C_2T_x$ flexible gas sensor still has a stable response of 9.68% to 500 ppm of NH_3 gas for 10 min at room temperature, and it is able to resist the change of response value caused by deformation well in the bending deformation range of -15°∼15°, and the response value is basically unchanged after 100 deformation cycles. The flexible sensor with $Ti_3C_2T_x$ as the flexible substrate has a good application prospect. It can be compounded with chemical production workshop operation clothes, work clothes, etc., so that it has a greater potential for application in the field of flexible wearable devices. An effective strategy is provided to promote the development of the new generation of intelligent flexible gas sensors and flexible electronic devices.

Keywords: $Ti_3C_2T_x$, gas sensor, flexible sensor, TPU fiber mat, gas-sensitive performance

Citation

Noam W Buckley (2023). Synthetic Textiles Processed Using Ionized Gas for Exterior Uses . Mari Papel Y Corrugado, 2023(1), 13–25.

1 Introduction

In 1934, Formalas invented and patented an experimental apparatus for the preparation of polymer fibers by electrostatic force. The patent announced how the polymer solution formed a jet between the electrodes, described in detail the use of high-voltage electrostatic force to prepare the fiber device, and was recognized as the beginning of fiber preparation by electrostatic spinning technology [1–3] However, when the electrostatic spinning technology first arose, it did not attract much attention. Until the middle of the 20th century, nanotechnology began to develop rapidly, nanomaterials are widely used in various fields, electrostatic spinning technology gradually received the attention of scholars from all walks of life and widespread concern [4–6] In terms of chemical and physical properties of polymer materials, electrostatic spinning is a technology that ultimately atomizes the precursor solution through an electric field. The precursor solution under the action of high voltage electric field, the polymer fluid does

Submitted: 19 December 2022
Accepted: 01 February 2023
Published: 01 April 2023

Vol. 2023, **No.** 1, 2023.

***Corresponding author:**
✉ Noam W Buckley
noamwbuckley@gmail.com

† Author read and approved the final version of the paper.

not operate in a liquid tiny form, but more in a form of atomization is implemented [7–9]

The process of electrostatic spinning can be described as the flow of a polymer solution in a strong electrostatic field. When the solvent is cured, a fibrous material is obtained. In the electric field, the fluid is atomized and finally transformed into fibers after running for a period of time and over a distance [10, 11] The world's earliest electrostatic spinning device is presented under the continuous research of the famous experts in the U.S., the test is placed in a high-voltage electric field with cellulose acetate solution as the precursor solution, respectively, the two electrodes are connected to the receiving device and the spinning head, when the electric field force overcomes the surface tension of the current, the small droplets will not be able to continue to maintain the original morphology of the original form, and thus the formation of the final bundled filaments, after curing fibers are formed. In subsequent studies and explorations, it has been found that the nature of the fluid employed in the experiment plays a crucial role in the success of spinning [12, 13] From the comprehensive development situation in recent years, the preparation method of electrostatic spinning has also been given strong attention and unprecedented importance in the preparation of nanomaterials. Electrostatic spinning is widely used in various fields because of the advantages of simple manufacturing device, low spinning cost, wide variety of spinnable substances, and controllable process. However, in the process of practical application, electrostatic spinning technology still has many problems. In the subsequent research process of electrostatic spinning, there is no in-depth penetration into the field of inorganic nanofibers to research. The finished inorganic nanofibers prepared by electrostatic spinning technology have insufficient flexibility and continuity, and are very brittle, therefore, in the specific use of the process, it will also bring a lot of inconvenience to the specific use [14, 15]

The application of electrostatic technology in textile is very wide, in addition to the prevention of static electricity in textile processing and anti-static treatment of products, but also in electrostatic spinning, electrostatic flocking, electrostatic method of nonwoven production and electrostatic electret product development and other aspects of a wide range of applications. Reasonable use of electrostatic technology, can design new textile processing methods, the development of functional textile products [16–18]

In this paper, textile-based flexible NH_3 gas sensors based on ionization gas sensors were prepared for external use. A $Ru/TiO_2/Ti_3C_2T_x$ flexible gas sensor based on MXene was prepared by compounding with $Ti_3C_2T_x$ to enhance the gas-sensitive response to NH3. Electrostatic spinning technology combined with hydrothermal method was introduced to prepare an electrostatically spun thermoplastic polyurethane fiber mat flexible multifunctional sensor based on TPU film. Characterization was carried out by XRD and SEM to verify the successful doping of nanoparticles as well as the successful synthesis of composites. The use of electrostatically spun TPU fibers randomly arranged to provide conditions for the penetration and entry of the composite material enhances the breathability of the sensor and makes the sensor more comfortable and skin-friendly. The prepared $Ru/TiO_2/Ti_3C_2T_x$-flexible gas sensors were thoroughly tested for their gas-sensitive properties, and the effects of various deformations on the gas-sensitive properties of the sensors were investigated.

2 Laboratory materials and equipment

2.1 Wearable Flexible Gas Sensors

2.1.1 Gas sensors

Gas sensor devices are mainly composed of two parts: the reactive material and the signal transmission. When the devices are in different kinds and different concentrations of gas environments, the chemical or physical responses of the gas sensor devices are expressed in various different forms of signals. According to the form of signal expression, gas sensors can be divided into different types.

Electrochemical gas sensors work on the principle that when a gas is detected, an electrochemical reaction occurs at the electrodes and an electrical signal is generated, e.g., a redox reaction causes a change in the electrical signal. As the concentration of the gas changes, the measured value of the electrical signal changes accordingly, obeying Faraday's law. The electrolyte is an important component of these sensors and is classified as neutral, acidic or alkaline depending on the pH range.

2.1.2 Gas Sensing Mechanisms of Gas Sensors

Gas sensors utilize changes in electrical performance parameters to achieve detection of target gases. Its gas-sensitive mechanism can be analyzed from a microscopic point of view and can be divided into the crystal boundary barrier control theory, electron

depletion layer (EDL) theory, hole accumulation layer (HAL) theory, Fermi energy level control theory and so on. That is, on the basis of changes in physical properties such as energy bands and work functions, changes in electrical performance parameters are induced. When analyzing the gas-sensitive mechanism from a macroscopic point of view, the main focus is on the effect of the gas on the gas-sensitive material. Currently, gas diffusion control, body resistance control, adsorption/desorption model and other gas-sensing mechanisms are frequently used. The different gas-sensing mechanisms are described below from a macroscopic perspective.

1. Gas diffusion control mechanism

   The factors that are emphasized in the gas diffusion control mechanism are the material's morphological characteristics and surface chemical reactions.

2. Body resistance control mechanism

   The principle of the body resistance control mechanism is the change in electrical resistance caused by the phase transition of the gas-sensitive material (certain metal oxide semiconductors).

3. Adsorption/desorption model

   Adsorption/desorption models can be divided into oxygen adsorption models, chemical adsorption/desorption models, and physical adsorption/desorption models.

2.1.3 *Flexible gas sensors*

Preparation of gas sensors on flexible substrates can fulfill some special application scenarios. Such gas sensors not only work normally when the substrate is flat, but also respond well to the target gas when the substrate deformation shows a curved state. With the development of wearable devices, portable devices and smart instruments in recent years, flexible gas sensors have been widely noticed.

Flexible gas sensors prepare gas-sensitive materials on flexible substrates with good mechanical properties, which are mainly categorized into plastic products, paper substrates, textile fabrics and so on.

Gas adsorption includes both chemical and physical adsorption. Physical adsorption relies on van der Waals forces, so that the gas molecules and the surface of the sensitive film to produce interaction forces, so as to adsorb gas molecules on the surface of the sensitive film Chemisorption is the exchange or transfer of electrons between the gas molecules and the material surface. Langemuir analyzed an equation (1) experimentally and analytically:

$$a = kp^{\frac{1}{n}}, \tag{1}$$

where a is the amount of gas molecules adsorbed by the sensitive film, p represents the partial pressure of the gas components in the gas phase at equilibrium, k represents a constant, and n represents a constant.

The solid-gas adsorption theory indicates that there are two scenarios that occur when gas molecules move with force against the surface of the film. One is that the gas molecules are ejected during the collision and no adsorption occurs. The other is that the gas binds to the film during the collision, and Van der Waals forces are generated, under which adsorption is formed, and three points are made about the pair model.

a. It can be adsorbed only when it touches the film vacancies.

b. The sensitive film surface is uniform.

c. Adsorption is a monomolecular layer.

Based on the above assumptions, Langmuir developed an isothermal gas adsorption equation (2):

$$a = A\frac{k_1 p}{k_2 + k_1 p}, \tag{2}$$

where a represents the amount of adsorbed gas, p is the partial pressure of the gas in the component, and A is the amount adsorbed at saturation. k_1 represents the adsorption rate of the gas, and k_2 represents the desorption rate of the gas. Based on Langemüller's theory, the BET adsorption theory was proposed by the scientific community. This adsorption theory can be expressed by the equation:

$$\frac{P}{V\left(P_0 - P\right)} = \frac{1}{V_M C} + \frac{C-1}{V_m C} * \frac{P}{P_0}, \tag{3}$$

where P is the partial pressure at which adsorption reaches equilibrium, P_0 is the saturated vapor pressure, V_m is the amount of gas required to cover the solid surface in a monolayer, V is the volume of adsorbed gas at the equilibrium pressure, and C denotes a constant related to adsorption.

2.1.4 *Textile-based flexible sensors*

Textiles, such as fiber yarns, play a key role in the development of human society and in everyday activities. Over the past two decades, a new generation of smart textiles - fiber yarns, nonwovens,

or fabrics with the ability to sense, drive, adapt, remember, communicate, and display - has gradually emerged. Particularly relevant are textile materials for personal health management, including personal health monitoring, precision targeted therapy, calorie and energy management. They are of interest because they can monitor vital sign signals, enhance physical comfort, and improve the quality of daily life.

1. Fiber yarn, as a textile with one-dimensional structure, has properties such as large specific surface area, light weight, softness, and breathability. What's more, fiber yarn has a rich pore structure, which can accommodate a large amount of conductive substances. Such as silver nanowires as a representative of the metal-based conductive materials, polyaniline as a representative of the conductive polymers and carbon nanotubes as a representative of the carbon-based materials, and ultimately produced fiber yarn-based flexible sensors, which are used in real-time monitoring of human vital signs signals and other fields. However, the cost of the functional materials used in the flexible sensor is high, resulting in low practical application value, and it is difficult to popularize.

2. Nonwoven fabrics have the advantages of light weight, softness and breathability of fiber yarns, and at the same time, they have a wider testing range and can fit the curvature of the human body during joint movement. After composite with conductive sensitive materials, it can be applied to the full range of human movement monitoring and biomedical and other fields.

   However, due to the nonwoven fabric is through the needle, hydroentanglement, electrostatic spinning, meltblown, hot melt method and other technologies, from the fiber into a network and then the fiber network reinforcement system. One of the fiber disorder arrangement, resulting in non-woven fabric-based flexible sensor in the external stimulus, the signal reception sensitivity of each point is different, the signal change is not stable, greatly hindering its finger bending, pulse monitoring and other human life characteristics of real-time signal monitoring applications.

3. Fabric is a flat and soft sheet obtained by crossing and knitting fiber yarns through weaving, knitting and other technical means, which has excellent softness and breathability, and is an ideal choice for the substrate material of flexible wearable sensors. Thanks to the orderly arrangement of internal fiber yarns, fabric-based flexible sensors can capture external stimuli with high sensitivity and precision. And rapidly transmit signals for effective monitoring of signals such as strain and temperature.

How to effectively construct conductive fabric-based flexible sensors, there are currently three main methods:

a. Using fabric as the substrate material, directly depositing conductive materials on the surface by means of transferring and coating.

b. Use fabrics such as silk cloth as the substrate material, and directly carbonize them to obtain intrinsically conductive fabrics.

c. First prepare conductive fiber yarn, and then as a weaving unit, through weaving, knitting and other techniques to construct conductive fabrics.

2.2 Design of flexible air-sensitive fabrics

Experiments will be conducted to prepare fabric electrodes for gas sensor substrates. Flexible gas sensors are prepared semiconductor gas-sensitive materials combined on the surface of the fabric electrode, through contact with the target gas, the fabric electrode resistance changes, and then determine the gas type, gas concentration and other information.

Therefore, the fabric electrode should have good electrical conductivity in addition to a certain stability, fatigue resistance and adsorption, to ensure that the material has good durability and sensitivity under the test conditions. And also consider the ease of combining gas-sensitive materials and the conductive stability after treatment.

What kind of physical and mechanical properties of the fabric sensor after screen printing treatment has a great relationship with its fabric material and fabric structure, so the design of the fabric electrode structure is related to the use of flexible gas sensors made of performance.

2.2.1 Selection of basecloth material

The selection of the base cloth material will have a certain impact on the sensitivity of the gas sensor, the use of durability, etc., so attention should be paid to the selection of the base cloth material:

1. The initial resistance of the selected base cloth should not be too large after processing, to prevent the preparation of the gas-sensitive element of the

initial resistance value is too large, the sensitivity and stability of the sensor test has an impact.

2. In order to extend the service life of the sensor, the selected base cloth material should be able to adapt to changes in the external environment, maintain good structural stability, thereby reducing its damage rate and extending its service life.

3. The base cloth material should have good adsorption properties so that as much gas-sensitive material as possible can be adsorbed on the surface of the base cloth. It can also make the combination of the material and the base cloth more solid and provide a guarantee for the subsequent measurement sensitivity.

First of all, between chemical fiber and natural fiber, chemical fiber has better physical and mechanical properties. And chemical corrosion resistance is strong, so chemical fiber is better than natural fiber in terms of stability and durability is a good choice for base cloth. But its disadvantage is poor anti-static ability, easy to pilling. Therefore, the focus is to choose a suitable chemical fiber as the base cloth material.

At present, polyester fiber is popular in the market, which is formed by spinning polyethylene terephthalate (PET) as raw material, and it is one of the most mature fibers in the current preparation technology. Polyester is a good choice for the base cloth because of its high strength, abrasion resistance, heat resistance and chemical resistance, which can meet the demand of long-term use.

Based on the above analysis, polyester fabric was chosen as the base fabric for the gas sensor in this experiment.

2.2.2 Selection of fabric organizational structure

Fabrics can be divided into woven fabrics, knitted fabrics and nonwoven fabrics according to the weaving method. Since knitted fabrics have greater elasticity and nonwoven fabrics have less strength, neither of them can meet the requirements of mechanical strength as the base material. Therefore, the experimental choice of woven fabrics as the experimental base cloth.

Woven fabric organization includes plain tissue, twill tissue, satin tissue and a series of changes in the organization. Among them, the plain weave tissue has the simplest structure but the strongest texture. The twill fabric has a softer texture, poorer stiffness and less strength due to the presence of interwoven warp and weft yarns. The satin fabric, which has the most complicated structure, has the worst strength due to the long floating lengths. Therefore, the simplest plain weave tissue is chosen as the base fabric tissue of the flexible gas sensor in the experiment.

3 Experimental procedures

3.1 Experimental reagents

The reagents used in the experiments in this paper are shown in Table 1.

3.2 Experimental apparatus

The apparatus in the experiments of this paper is shown in Table 2.

3.3 Manufacture of flexible multifunctional sensors

3.3.1 Less-layer $Ti_3C_2T_x$ preparation

In this paper, the same LiF/HCl method was used to etch the MAX phase to prepare the oligolayer $Ti_3C_2T_x$.

First, 3.6 g LiF was weighed and added to 50 ml of 9 mol/l hydrochloric acid and stirred (20 min) at 1000 r/min until all dissolved. Then 3g of MAX phase was weighed and added slowly (about 30min) to the mixed solution and stirred by heating at 50°C for 24h at 600r/min.

After stirring was completed, the black mixed suspension was removed into a 60 ml centrifuge tube and centrifuged with deionized water at 3500 r/min.

Repeat the centrifugation process until the upper suspension was colloidal, remove the upper black colloidal dispersion and sonicate it in an ultrasonic cleaner for 2 h. After sonication, put it into a centrifuge tube and centrifuge it at 3500 r/min for 1h.

Finally, the upper layer of black colloid was removed and freeze-dried for 10 h. The black powder obtained by grinding was the lesser layer $Ti_3C_2T_x$. All the above experiments were carried out in PTFE beakers.

3.3.2 Preparation of TiO2/Ti3C2Tx

60 mg of less layer $Ti_3C_2T_x$ was added to 30 ml of deionized water and sonicated for 30 min to obtain a homogeneous mixed dispersion. After that, the dispersion was put into a 30 ml hydrothermal reactor and put into a drying oven for hydrothermal reaction at 180°C for 10 h. The naturally cooled dispersion was put into a petri dish and freeze-dried for 10 h. Finally, the dried material was milled, and the powder obtained was the $TiO_2/Ti_3C_2T_x$ composite material.

Drug name	Drug purity	Producer
MAX phase	98%	Jilin province 11 technology co., LTD
HC1	37.8%	Shanghai Aladdin biochemical technology co., LTD
LiF	Analytical purity	Shanghai Aladdin biochemical technology co., LTD
$RuC1_3 \cdot 3H_2O$	97%	Shanghai Aladdin biochemical technology co., LTD
TPU grain	100%	Shanghai meisheng plastic co., LTD
Ammonia water	Analytical purity	Shanghai Aladdin biochemical technology co., LTD
Anhydrous ethanol	Analytical purity	National drug collectivization co., LTD
Dimethyl methylamine	Analytical purity	National drug collectivization co., LTD
Formaldehyde	Analytical purity	National drug collectivization co., LTD
Acetone	Analytical purity	National drug collectivization co., LTD
Methyl alcohol	Analytical purity	National drug collectivization co., LTD
Deionized water	Analytical purity	Laboratory self-control

Table 1. Laboratory reagent

Instrumentation	Type	Producer
Constant temperature magnetic stirrer	HSC-19T	Ningbo yinzhou group an experimental instrument co., LTD
High speed centrifuge	4-20R	Hunan hengno instrument equipment co., LTD
Electric drum drying box	PHG-9036A	Shanghai jinghong experimental equipment co., LTD
Vacuum oven	DZF-6050AB	Zhengzhou shengyuan instrument co., LTD
Ultrasonic cleaning machine	G-100ST	Shenzhen song energy cleaning equipment co., LTD
Microelectronic balance	HZK-FA110	Fuzhou hua zhi science instrument co., LTD
Electrostatic spinning equipment	ET-2535H	Beijing yongkang technology development co., LTD
Flexible electronic device testing platform	AES-4SD	Beijing zhongke technology co., LTD
Contact Angle measuring instrument	DSA-100	Germany kruss

Table 2. Laboratory instrument

3.3.3 Preparation of Ru/TiO2/Ti3C2Tx composites

Firstly, 60 mg of $TiO_2/Ti_3C_2T_x$ powder was weighed into a glass beaker of 10 ml of deionized water and sonicated for 30 min to obtain a homogeneous dispersion. Then 0.5, 0.6 and 0.7 ml of $RuC1_3 \cdot 3H_2O$ solution with a concentration of 0.1 mol/l were added to the beaker respectively, and the solution was magnetically stirred at 600 r/min for 30 min to make it fully reduced. Different proportions of $Ru/TiO_2/Ti_3C_2T_x$ composites can be obtained.

3.3.4 Preparation of TPU fiber mats

First, 15 ml of DMF and THF were measured respectively and the two solutions were mixed well. Then 6.3 g of TPU particles were weighed and added into it, and stirred at room temperature for 5 h to obtain a homogeneous TPU precursor solution.

The electrostatic spinning equipment was set at 50°C for preheating to maintain a stable temperature, after which 12 ml was extracted with a 20 ml syringe for electrostatic spinning, and the obtained film was dried at room temperature for 10 h and cut into long strips of 6 cm in length and 1 cm in width, which can be used to obtain the TPU film.

The parameters of the electrostatic spinning machine were set as follows: spinning distance of 20cm, voltage of 20kv, syringe push speed of 5ml/h, left and right translation distance of 150mm, drum speed of 100rpm.

3.3.5 $Ru/TiO_2/Ti_3C_2T_x$ Preparation of flexible multifunctional sensors

The cut TPU films were put into different proportions of the dispersion and ultrasonicated at 1200 W for 2 h. The ultrasonicated films were then washed with deionized water to remove the excess material from the surface, and then the films were vacuum dried at 60 °C for 10 h to obtain the $Ru/TiO_2/Ti_3C_2T_x$-flexure sensors.

For different ratios were named MXene/$TiO_2/Ru-0.5$, MXene/$TiO_2/Ru-0.6$, MXene/$TiO_2/Ru-0.7$ respectively.

4 Testing and characterization

4.1 Morphological characterization of fibers (SEM)

The samples of nanofiber membranes were fixed with conductive adhesive on the sample stage for gold spraying treatment, and then the surface morphology of each nanofiber membrane was observed by scanning

electron microscope at an accelerating voltage of 10 KV using the Feiner Benchtop from Feiner, the Netherlands.

4.2 X-ray diffraction tests (XRD)

A Bruker D8 Advance X-ray diffractometer was used to determine the crystalline phase of $Ru/TiO_2/Ti_3C_2T_x$ nm fiber membranes. The diffraction target tested was $CuK\alpha$, with an angle range of 15°-80°, a step size of 0.04° and a scanning rate of 0.3 s/step.

4.3 Transform Infrared Spectroscopic Testing (FTIR)

A Nicolet iS50 Fourier Transform Infrared (FTIR) spectrometer from Thermo Fisher Scientific was used for infrared characterization testing of each nanofiber membrane. The wavelength range of the test was 4000-400cm^{-1} with a resolution of 0.08cm^{-1}.

4.4 Gas Sensitive Performance Testing

The gas-sensitive properties of PEDOT/composite conductive woven fabrics were tested using the WS-30B Gas Sensitive Element Test System from Zhengzhou Weisheng Electronic Technology Co.

The sensor device was operated at a voltage of 6V. By choosing a suitable load card, the baseline was made to proceed smoothly at the middle position of 0-1. After about 3 min, the gas or liquid to be detected is injected in the corresponding part of the instrument and the change in resistance is measured using the configured serial probes, respectively.

The gas-sensitive performance of the gas-sensitive materials was evaluated by key parameters of sensitivity, selectivity and stability. It is not easy to obtain due to the limitation of purchasing gases.

Therefore, the gas sensing performance was investigated in this experiment using alcohol as the detection gas. The gas distribution equations for measuring gases are as follows:

$$Vx = V \times C \times 10^{-6} \times \frac{29^3 + Tr}{29^3 + Tb}. \tag{4}$$

The gas injection volume (V_x) is calculated in milliliters (ml) according to equation (4).

$$Vx = \frac{V \times C \times M}{256 \times D \times P} \times 10^{-9} \times \frac{29^3 + Tr}{29^3 + Tb}. \tag{5}$$

When measuring liquid vapor, the liquid vapor injection volume (V_x) is calculated according to equation (5) in milliliters (ml).

Equation (4), (5), V is the volume of the test box, the unit is milliliter (ml). C is the liquid vapor concentration in parts per million (ppm). M is the molecular weight of the liquid (g), D is the specific gravity of the liquid in grams per cubic centimeter (g/cm3). P is the purity of the liquid, Tr is the room temperature in degrees Celsius (℃). Tb is the temperature inside the test chamber box in degrees Celsius (°C). The percent sensitivity of the gas sensor is generally expressed as S using the ratio of resistance before and after the test:

$$S = (Rg - Ra)/Ra \times 100\%, \tag{6}$$

where, Ra is the resistance value of the gas-sensitive element in air. Rg the resistance value of the gas-sensitive element in the test gas.

5 Results and discussion

5.1 Micro-morphological observation and analysis

The sensitive performance of flexible humidity sensors is closely related to the microscopic morphology of the film surface. Therefore, in this subsection, SEM, XRD, and FTIR characterization methods are used to observe and analyze the micro-morphology of the prepared sensitive films.

The surface of the sensitive films prepared by electrostatic spinning was firstly observed and analyzed morphologically by SEM and XRD methods. SEM obtained by depositing a mixture of $Ti_3C_2T_x$ and TiO_2 onto a PET substrate using electrostatic spinning. It can be seen that $Ti_3C_2T_x$ of the electrostatically spun filament has good contact with the flexible substrate and the metal electrodes, and the overall spraying is good, no agglomeration is generated, and there are localized artificial residues. The carbon nanotubes are well distributed on the substrate and a large number of carbon nanotubes are in contact with each other. This indicates that the flexible carbon nanotubes prepared by the electrostatic spinning process have good microscopic properties.

The XRD diffraction patterns of $Ti_3C_2T_x$, TiO_2 and $Ru/TiO_2/Ti_3C_2T_x$ are shown in Figure 1.

$Ti_3C_2T_x$ The 2θ of the pattern shows bun peaks at 11.25° and 21.68°, which are typical diffraction peaks of PVP amorphous polymers. Two diffraction peaks of carbon nanotubes appeared at 27.14° and 43.05°, respectively.

After the formation of the mixture of $Ru/TiO_2/Ti_3C_2T_x$, all the diffraction peaks are

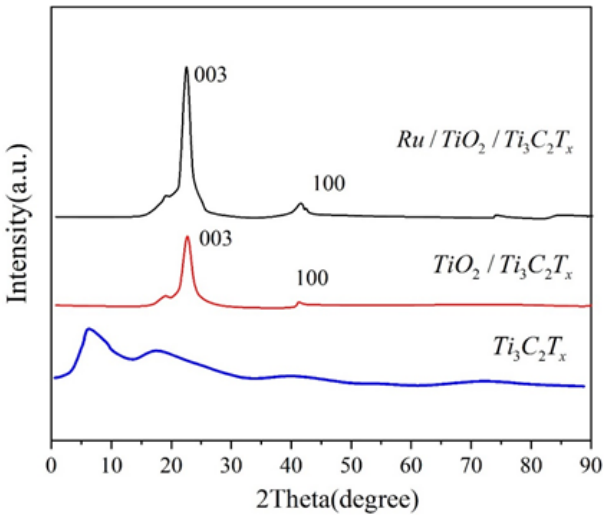

Figure 1. $Ti_3C_2T_x$ $TiO_2$and $Ru/TiO_2/Ti_3C_2T_x$ diffraction pattern

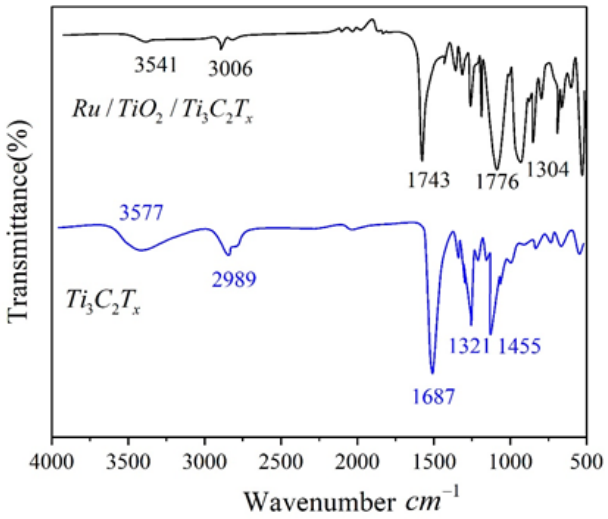

Figure 2. $Ti_3C_2T_x$ and $Ru/TiO_2/Ti_3C_2T_x$ the spectrogram

the diffraction peaks of nanotubes, indicating that their $Ti_3C_2T_x$ diffraction peaks are weak and masked by them. Meanwhile, the crystal peaks at (003) and (100) increased in strength, indicating that its $Ti_3C_2T_x$ modification changed the stacking orientation of multiwalled carbon nanotubes, which led to an increase in the crystal surface burst at (003) and (100).

In order to further characterize and analyze the films in this paper Fourier Transform Infrared (FTIR) spectroscopy was also done. The FTIR spectra of $Ti_3C_2T_x$, TiO_2 and $Ru/TiO_2/Ti_3C_2T_x$ composites are shown in Figure 2. $Ti_3C_2T_x$ The characteristic peak of the stretching vibration of -OH is at 3577 cm^{-1} in the infrared spectrum, and the peak corresponding to 2989cm^{-1} is from the stretching vibration of -CH3 in $Ti_3C_2T_x$. There is a strong absorption peak at wavelength 1687cm^{-1}, which is recognized as the absorption peak caused by the stretching vibration of the carbonyl group (C=O) in the TiO_2 ring of $Ti_3C_2T_x$. 1321cm^{-1} and 1455cm^{-1} show absorption peaks, which is the absorption peak of the stretching vibration of the C-N bond in $Ti_3C_2T_x$.

$Ti_3C_2T_x$ After TiO_2 modification, the absorption peaks at 3541cm^{-1}, 3006cm^{-1}, and 1743cm^{-1} were shifted. At the same time, a new absorption peak was generated at 1304cm^{-1}, caused by the C-O-C stretching vibration peak. It indicates that $Ti_3C_2T_x$ and TiO_2 combined with each other to produce a new crystalline product.

5.2 SEM characterization of thin films

In this subsection, SEM characterization of TPU film, $Ti_3C_2T_x$ film, $TiO_2/Ti_3C_2T_x$ layered film and $Ru/TiO_2/Ti_3C_2T_x$ composite film is carried out to obtain their film surface morphology.

It can be seen that $Ti_3C_2T_x$ film shows a more uniform rough surface. The surface morphology of the $TiO_2/Ti_3C_2T_x$ layered film is very similar to that of the prepared pure TPU film, with the presence of holes of different sizes on the surface. A small amount of graphene can also be seen, and the graphene clusters are distributed on the substrate, making the TPU does not cover it completely.

SEM characterization can clearly see the morphology of graphene, which is due to the fact that graphene is located on top of the TPU. Due to the small amount of graphene, it also cannot cover the TPU film. Comparing the surface morphology of the above three, it is found that the composite film has the densest distribution of voids, thus providing more adsorption sites for nitrogen dioxide gas, enhancing the gas-sensitive response and improving the sensitivity.

5.3 Flexible sensor gas sensitivity

The prepared $Ru/TiO_2/Ti_3C_2T_x$ flexible gas sensors were comprehensively tested for their gas-sensitive properties, and the effects of various deformations on the gas-sensitive properties of the sensors were investigated.

Considering the susceptibility of $Ti_3C_2T_x$ to pyrolysis at 201 °C and the practicality of flexible gas sensors, room temperature was chosen as the operating temperature of the gas-sensitive element to explore its application as a gas sensor at room temperature. No heating resistor was added to the gas-sensitive element, and all tests were done at room temperature. In

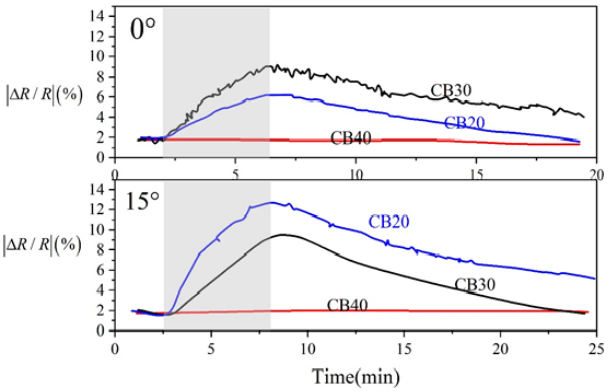

Figure 3. $Ti_3C_2T_x$ dynamic response curve

addition, considering the actual use of the gas-sensitive element, the response time was set to 10 minutes to test the response of the gas sensor to 500 ppm NH_3 within 10 minutes.

Firstly, in order to select the flexible substrates with suitable conductivity, carbon black with different mass fractions was added to methyl vinyl silicone rubber to prepare flexible substrates with different conductivity, labeled as CB20, CB30, and CB40, and the gas-sensitive elements were prepared respectively.

$Ti_3C_2T_x$ The dynamic response curves are shown in Figure 3, which illustrates the response of $Ti_3C_2T_x$ with different flexible substrates in 500 ppm NH_3 gas and after applying a 15° deformation. Without external force applied, $Ti_3C_2T_x$ the sensor prepared with the flexible substrate of CB20 has a 12.3% response to 500 ppm NH_3 but the response value decreases significantly after applying a 15° bending deformation. This may be due to the presence of small cracks in the $Ti_3C_2T_x$ sensing layer, and the higher resistance of the flexible substrate CB20 directly affects the response value.The response value of the sensor with CB40 as the flexible substrate is insignificant with or without the applied deformation, probably because the resistance of the flexible substrate is too small, and the change in the resistance of the sensing layer does not have much effect on the resistance of the sensor as a whole.

In contrast, in the $TiO_2/Ti_3C_2T_x$ sensor, the response value after applying a 15° bending deformation was essentially the same as the response value under no deformation. Therefore, CB30 was chosen as the flexible substrate to further explore its gas-sensitive performance.

Gas sensing tests without deformation were performed on the devices of CB30 to examine their gas-sensitive performance without applying any deformation. The sample gas sensing test is shown in Figure 4.

The cyclic dynamic response curve of the sample sensor to 500 ppm NH_3 is shown in Figure 4(a), $Ti_3C_2T_x$/CB30 can show good cyclic stability under the cyclic cycle test of 500 ppm of NH_3 gas, and can achieve a response value of 9.68% within a response time of 5 minutes.

It was then tested for a NH_3 gas concentration gradient, and Figure 4(b) shows the dynamic response curve of $Ti_3C_2T_x$/CB30 to 100-500 ppm of NH_3 with a linear fit.

The fitting results are shown in Figure 4(c), and it can be found that the response of NH_3/CB30 to $Ti_3C_2T_x$ gas has a good linear relationship with concentration, with a sensitivity S of 0.0268% ppm^{-1} and a correlation coefficient R^2 of 0.9949.

The effect of bending deformation on the response value of $Ti_3C_2T_x$/CB30 was then explored. The gas detection performance of the $Ti_3C_2T_x$/CB30 gas sensor is shown in Figure 5.

The changes in the response value of the gas-sensitive element for different bending deformations are shown in Figure 5(a) to (d). It can be found that no matter bending upward or downward, the response value is not much affected in the case of smaller deformation of 15°, while in the case of bending deformation of 30°, the response value is decreased in different degrees. The decrease in the response of the downward bending 30° sensors may be due to more cracks in the sensing layer at the microscopic level, resulting in an increase in resistance, while the flexible substrate does not participate in the gas response, and this part of the resistance did not increase after the passage of the gas, resulting in a decrease in the overall response. A decrease in the response of the sensors bent upwards by 30° also occurred, possibly due to the increase in overall resistance of the sensing layer and the flexible substrate due to the larger deformation and a possible decrease in the rate of gas desorption on the surface of the material due to the bending of the sensing layer.

The response value of $Ti_3C_2T_x$/CB30 to NH_3 gas is plotted against the angle of the applied bend (e). It is clearly shown that the response value is essentially constant in the range of bending angles from -15° to 15°, while the response value decreases when the bending angle is too large.

In order to investigate the actual flexible application of $Ti_3C_2T_x$/CB30 in the range of small bending angles,

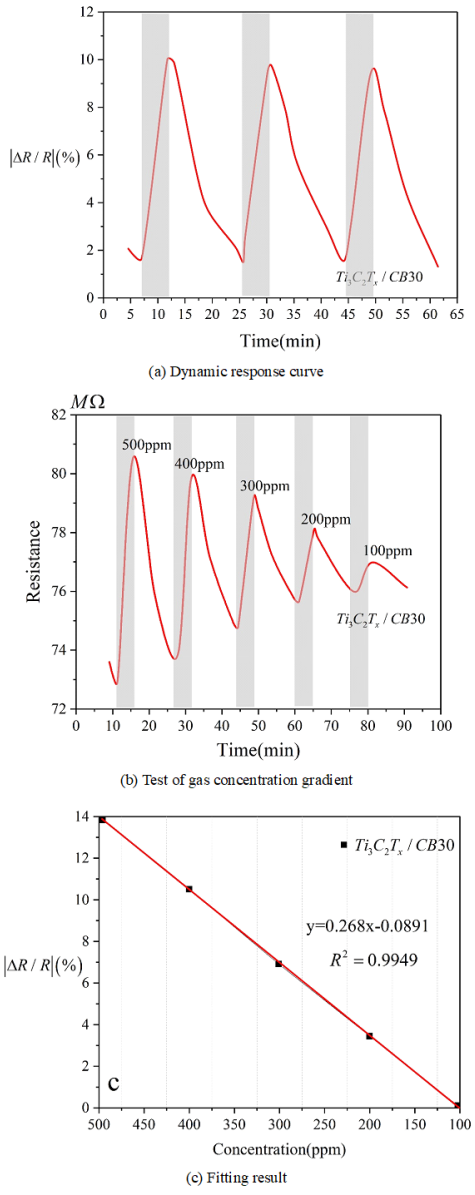

Figure 4. Sample gas sensing test

the gas sensor was repeatedly bent 100 times from -15° to 15°, and then the response was tested. The test results are shown in Figure 5(e), and the response value is basically unchanged.

The reason for the slight decrease may be related to the loss of $Ti_3C_2T_x$/CB30 during bending and the decrease in the response value of the $Ti_3C_2T_x$/CB30 material itself under the influence of water molecules in the air. This suggests that $Ti_3C_2T_x$/CB30 is able to maintain the stability of its gas-sensitive properties at bending angles in the range of -15° to 15°. At larger bending angles, it can also have a certain detectable air-sensitive signal.

Although $Ti_3C_2T_x$/CB30 performs well in the cyclic cycle test, its sensing layer is a conductive MOFs material, which is more sensitive to water molecules in the air, and may cause an increase in the sensor's overall resistance baseline or a decrease in the response value, which leads to a reduction in its actual service life, and has a certain impact on the value of the use of flexible sensors.

In summary, the $Ti_3C_2T_x$/CB30 gas sensor is able to provide a good and stable response to NH_3 in gas detection performance. In the deformation test, it can maintain a stable response to the target gas under the bending deformation of -15°∼15°. The /CB30 gas sensor has a good value in the detection of NH_3 gas at room temperature with small angle deformation.

5.4 Mechanical properties

The tensile test properties of pure TPU, $Ti_3C_2T_x$, $TiO_2/Ti_3C_2T_x$ and $Ru/TiO_2/Ti_3C_2T_x$ were tested.

The stress-strain curves of the samples are shown in Figure 6. These four samples exhibited similar mechanical behavior characteristics, showing similar linear and yield regions in the typical stress-strain curves.The breaking strengths of TPU, $Ti_3C_2T_x$, $TiO_2/Ti_3C_2T_x$ and $Ru/TiO_2/Ti_3C_2T_x$ were 42.172 MPa, 46.707 MPa, 49.046 MPa and 50.299 MPa, respectively.In addition, their breaking strains were 71.13%, 80.05%, respectively, 89.93% and 99.69%.

From the data analysis, it can be seen that the ultimate stress as well as the strain at break of the original yarns were not reduced but enhanced after various treatments, and they still have the excellent mechanical strength and flexibility of the original core yarns. This may be attributed to the interaction force between the nanofibers in the sensor skin and the core yarn which resulted in the increased tensile resistance of the yarn

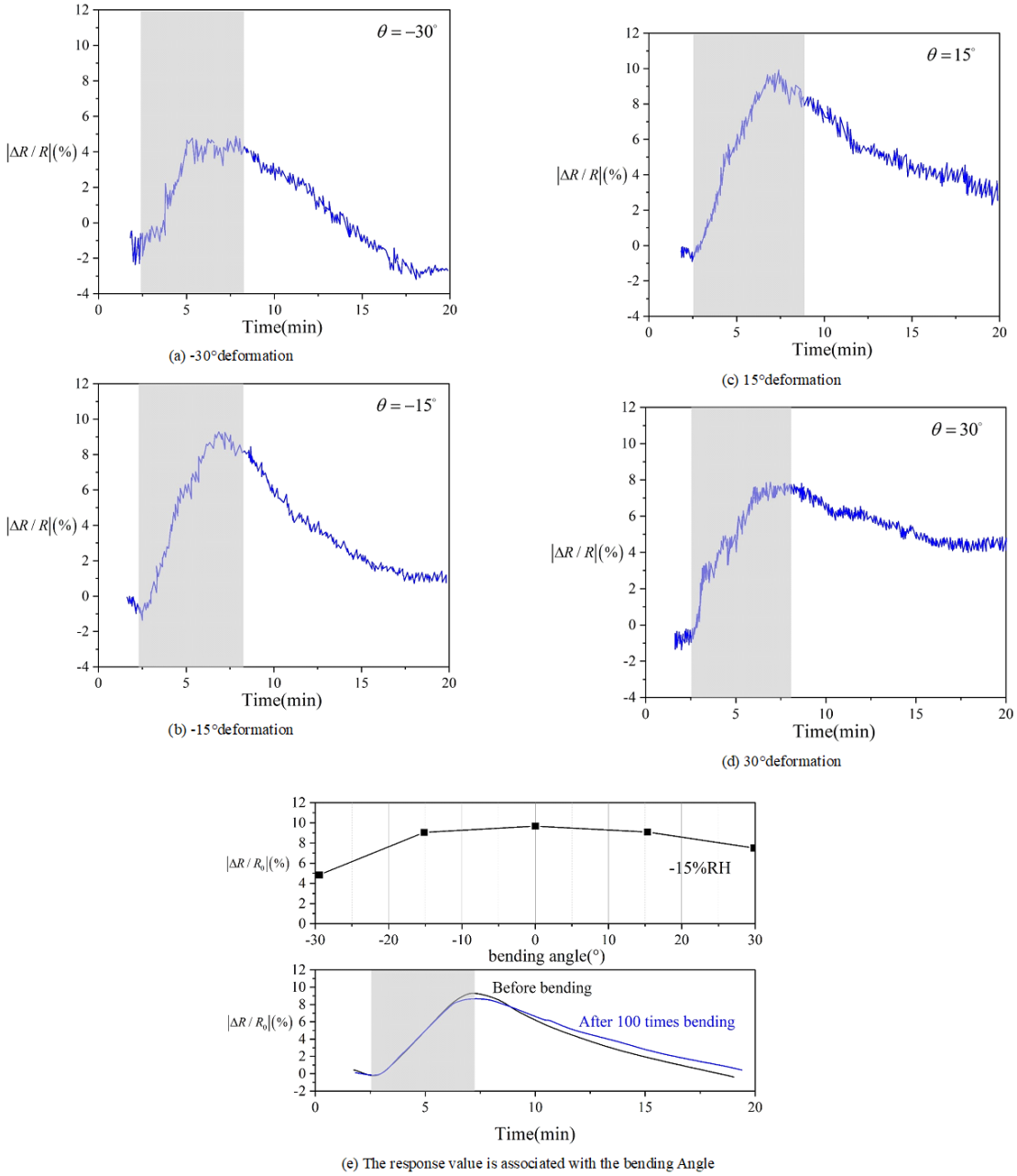

Figure 5. $Ti_3C_2T_x$/CB30 Gas detection performance of gas sensors

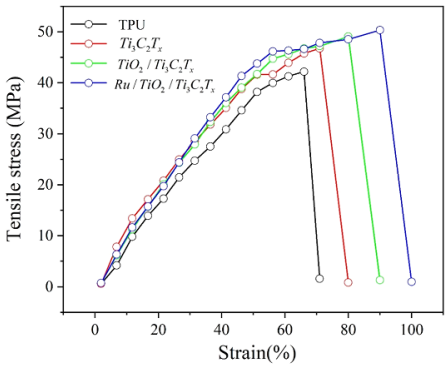

Figure 6. The stress-strain curve of the sample

sensor.

The loading of $Ti_3C_2T_x$ particles with ZnO/SnO2 nanomaterials makes the surface of nanofibers rougher, further increasing the interaction force between the two. This also verifies that the $Ru/TiO_2/Ti_3C_2T_x$ sensor possesses the relevant performance characteristics of yarn, which has potential applications in the wearable field.

6 Conclusion

In this paper, ionization gas sensors are used to design wearable textile-based flexible sensors based on two-dimensional material $Ti_3C_2T_x$, and the MAX phase is etched by LiF/HCl method to prepare less layer $Ti_3C_2T_x$, and composites are prepared by using MXene material properties. Gas sensors were prepared for composite material $Ru/TiO_2/Ti_3C_2T_x$ and their gas-sensitive properties were investigated.

1. Scanning electron microscopy obtained by depositing a mixture of $Ti_3C_2T_x$ and TiO_2 onto a PET substrate using the electrostatic spinning technique. The electrostatically spun $Ti_3C_2T_x$ has good contact with the flexible substrate and the metal electrodes with good overall coating. It indicates that the flexible carbon nanotubes prepared by the electrostatic spinning process have good microscopic properties.

2. A room-temperature environment was set up to exclude the addition of a heating resistor to the gas-sensitive element, and the response of $Ti_3C_2T_x$ with different flexible substrates to 500 ppm NH_3 was determined, as well as the response after applying a deformation of 15°. Without applying an external force, $Ti_3C_2T_x$ the sensor prepared with the flexible substrate of CB20 has a 12.3% response to 500 ppm NH_3.

3. Gas sensing tests on $Ti_3C_2T_x$/CB30 with invariant variations, the response of $Ti_3C_2T_x$/CB30 to NH_3 gas had a good linear relationship with concentration, with a sensitivity S of 0.0268% pp m^{-1} and a correlation coefficient R^2 of 0.9949.

4. Examination of the effect of different bending deformations on the response values of $Ti_3C_2T_x$/CB30 shows that, in the case of smaller deformations of 15°, the two cases of upward bending or downward bending do not have much effect on the response values of $Ti_3C_2T_x$/CB30. However, in the case of 30° bending deformation, the response values were decreased to different degrees. And the results of the mechanical properties of the flexible sensors indicate that the nanofibers of the sensor cortex and the core yarn generate interaction forces that make the yarn sensor more resistant to stretching. The mechanical properties of the $Ru/TiO_2/Ti_3C_2T_x$ flexible gas sensors were enhanced and thus have potential applications in the wearable field.

References

[1] Komolafe, A., Zaghari, B., Torah, R., Weddell, A. S., Khanbareh, H., Tsikriteas, Z. M., . & Beeby, S. (2021). E-textile technology review–from materials to application. *Ieee Access*, *9*, 97152-97179.

[2] Persson, N. K., Martinez, J. G., Zhong, Y., Maziz, A., & Jager, E. W. (2018). Actuating textiles: next generation of smart textiles. *Advanced Materials Technologies*, *3*(10), 1700397.

[3] Takeshita, T., Yoshida, M., Takei, Y., Ouchi, A., Hinoki, A., Uchida, H., & Kobayashi, T. (2019). Relationship between contact pressure and motion artifacts in ECG measurement with electrostatic flocked electrodes fabricated on textile. *Scientific Reports*, *9*(1), 5897.

[4] Wang, L., Fu, X., He, J., Shi, X., Chen, T., Chen, P., . & Peng, H. (2020). Application challenges in fiber and textile electronics. *Advanced Materials*, *32*(5), 1901971.

[5] Mokhtari, F., Cheng, Z., Raad, R., Xi, J., & Foroughi, J. (2020). Piezofibers to smart textiles: A review on recent advances and future outlook for wearable technology. *Journal of Materials Chemistry A*, *8*(19), 9496-9522.

[6] Chen, J., Guo, H., Pu, X., Wang, X., Xi, Y., & Hu, C. (2018). Traditional weaving craft for one-piece self-charging power textile for wearable electronics. *Nano Energy*, *50*, 536-543.

[7] Zhou, F. L., & Gong, R. H. (2008). Manufacturing technologies of polymeric nanofibres and nanofibre yarns. *Polymer International*, *57*(6), 837-845.

[8] Wen, J., Xu, B., Gao, Y., Li, M., & Fu, H. (2021). Wearable technologies enable high-performance

textile supercapacitors with flexible, breathable and wearable characteristics for future energy storage. *Energy Storage Materials, 37*, 94-122.

[9] Malwade, S., Abdul, S. S., Uddin, M., Nursetyo, A. A., Fernandez-Luque, L., Zhu, X. K., ... & Li, Y. C. J. (2018). Mobile and wearable technologies in healthcare for the ageing population. *Computer Methods and Programs in Biomedicine, 161*, 233-237.

[10] Shi, J., Liu, S., Zhang, L., Yang, B., Shu, L., Yang, Y., . & Tao, X. (2020). Smart textile-integrated microelectronic systems for wearable applications. *Advanced Materials, 32*(5), 1901958.

[11] Simegnaw, A. A., Malengier, B., Rotich, G., Tadesse, M. G., & Van Langenhove, L. (2021). Review on the Integration of Microelectronics for E-Textile. *Materials, 14*(17), 5113.

[12] Dong, K., Hu, Y., Yang, J., Kim, S. W., Hu, W., & Wang, Z. L. (2021). Smart textile triboelectric nanogenerators: Current status and perspectives. *MRS Bulletin, 46*(6), 512-521.

[13] Ramachandran, V., Shintake, J., & Floreano, D. (2019). All-fabric wearable electroadhesive clutch. *Advanced Materials Technologies, 4*(2), 1800313.

[14] Mishra, R., & Militky, J. (2018). Nanoparticles and textile technology. *Nanotechnology in Textiles: Theory and Application, 181*.

[15] Lund, A., Darabi, S., Hultmark, S., Ryan, J. D., Andersson, B., Ström, A., & Müller, C. (2018). Roll-to-roll dyed conducting silk yarns: a versatile material for e-textile devices. *Advanced Materials Technologies, 3*(12), 1800251.

[16] Yuce, I., Yukseloglu, M., & Canoglu, S. (2018). An analysis of conductive fibers as smart textiles. Annals of the University of Oradea. *Fascicle of Textiles, Leatherwork, 19*(2), 105-110.

[17] Huang, R., Zhang, S., Zhang, W., & Yang, X. (2021). Progress of zinc oxide-based nanocomposites in the textile industry. *IET Collaborative Intelligent Manufacturing, 3*(3), 281-289.

[18] Dong, K., Peng, X., Cheng, R., & Wang, Z. L. (2022). Smart textile triboelectric nanogenerators: prospective strategies for improving electricity output performance. *Nanoenergy Advances, 2*(1), 133-164.